Original Research Article

J. Funct. Mater. Biomol. 10 (1) (2026) pp 1201-1210

SACRED HEART RESEARCH PUBLICATIONS

Journal of Functional Materials and Biomolecules

Journal homepage: www.shcpub.edu.in

ISSN: 2456-9429

Structural, magnetic, and electrochemical investigations of $NiFe_2O_4$ nanoparticles for microelectronic applications

R. Ramesh, and D. Lakshmi*

Received on 17 April 2026, accepted on 27 May 2026,

Published online on June 2026

Abstract

In this study, we report the synthesis of $NiFe_2O_4$ prepared by a one-step chemical route method. X-ray diffraction analysis revealed the cubic phase structure of the prepared sample, and the average size was found to be 47 nm. The surface morphology of the $NiFe_2O_4$ nanoparticles calcinated at 800 ºC was analysed using SEM studies and showed homogeneous distribution of large and tiny-sized spherical-shaped nanoparticles with few agglomerates. The formation of Ni and Fe-O was confirmed by the strong absorption peaks at 549.11 cm^{-1} and 466.66 cm^{-1} obtained using FTIR spectroscopy. The optical bandgap of the synthesised $NiFe_2O_4$ nanoparticles was estimated as 5.22 eV. The electrochemical performance of the synthesised $NiFe_2O_4$ nanoparticles with applied frequency at various temperatures was analysed using dielectric measurements. The magnetic property of the sample was studied using VSM studies.

Keywords: Chemical synthesis, Nickel Ferrite, Dielectric, Magnetic properties, Electron microscopy.

1. Introduction

In the past few decades, there has been a substantial improvement and innovation made in the preparation of ferrite materials for numerous applications. Preparing a single compound of nanoparticles like CuO, ZnO, NiO, FeO, etc., has only a limited application. If these compounds are grouped by means of physical, chemical, electrochemical, or by some other means of techniques as a complex formation of ferrites, it becomes more effective in terms of the enhanced properties, including magnetic, dielectric behaviour, etc. [1]. There are reports available on the synthesis of nickel ferrites by various methods for a focused application in the field of nanotechnology, medicine, drug delivery, etc. In general, nickel ferrite is a multifunctional material because of its ferromagnetic property and high electrochemical stability; it was used in magnetic-based measuring devices. Because of its superparamagnetic behaviour, it was used in magnetic fluids, photo magnetic materials and microwave devices [2]. The behavior and property of the material can be varied based on the method of preparation and annealing temperature for instance, a study on the influence of the preparation method in the structural and magnetic properties of nickel ferrite by sol-

***Corresponding author:** E-mail: rramesh@shctpt.edu
Affiliation: Department of Physics, Sacred Heart College (Autonomous), Tirupattur-635 601, Tamil Nadu, India.

gel and co-precipitation method revealed the difference in the magnetic behavior of the sample annealed at 400 ºC and 600 ºC temperatures posed super paramagnetic and lesser sized ferromagnetic performance [3]. A report on nickel ferrite -SiO_2/Ag core/shell nanocomposites exhibited a stable electrochemical behaviour [4]. An investigation of annealing temperatures for controlling the particle size of nickel ferrite compound synthesised by the wet chemical route was reported [5]. Usually, a single metal-based metal oxide was applied for the plant growth to improve the crop productivity. Some of the notable toxic metal oxides are iron oxides, zinc oxide, nickel oxide, and boron-related. In a recent study, green synthesis of zinc ferrite mediated by Petroselinum Cripsum was reported, and the synthesised sample was tested in plant species like wheat, Triticum Vulgare. L and found that application of zinc ferrite on these plant species showed a lower cytotoxicity [6]. The effect of calcination temperature also plays a vital role in modifying the size and shape of the particles to be prepared [7]. If the calcination temperature is low, there is a possibility of the addition of contaminants /impurities from the starting organic/ inorganic materials, which reduces the reactivity of the particle, and it has been reported in the literature [8]. All these available studies give the impression that bimetallic oxides can be produced by various methods and processes, which can alter or modify the properties of the desired sample and which can be used for various applications based on their enhanced properties. Here in this experimental study, we report the one-step chemical route synthesis of nickel ferrite nanoparticles for microelectronic applications. The results obtained based on the magnetic measurements by VSM analysis and the optical and dielectric measurements performed in this sample exhibit its ability to be used in microelectronic devices.

2. Experimental Procedure

2.1. Materials and Method

In this experimental study, the method utilised is a one-step chemical route in which the starting materials solution was prepared separately using distilled water, sulphuric acid, and mixed straight to initiate the reaction process. Nickel nitrate hexahydrate and iron oxide were used as the precursor and the dopant material to synthesize nickel ferrite, and no precipitating agent was used in this study.

2.2 Synthesis of $NiFe_2O_4$ nanoparticles

$NiFe_2O_4$ nanoparticles were prepared by a direct one-step chemical route method. One mole of nickel nitrate was dissolved in distilled water to prepare a 0.5 mole iron oxide solution, which was mixed and stirred well in a magnetic agitator for 6 hours in the laboratory at ambient temperature. The pH of the solution mixture was maintained at 10 to get the desired morphology of the sample as per the previous literature. After continuous stirring, a dark brownish-colored sediment was observed. The liquid precipitate with a pale brown colored solution was centrifuged at 10000 rpm, washed thrice with deionised water to eliminate the impurities produced during preparation. The centrifuged sample was kept in the hot air oven for 4 hours at 180 °C for the drying

process. The dark reddish-brown powder obtained from the sample was calcinated in the furnace at 800 °C for 4 hours. The final powder was ground to a uniform size and used for the characterisation studies.

3. Results and Discussion

3.1. X-ray diffraction studies

$NiFe_2O_4$ nanoparticles prepared by the one-step chemical route method were examined for their structural characteristics by using an X-ray diffractometer in the 2θ range 10° to 80°. The obtained pattern of the XRD with good intensities of strong diffractions of the $NiFe_2O_4$ is shown in Fig. 1.

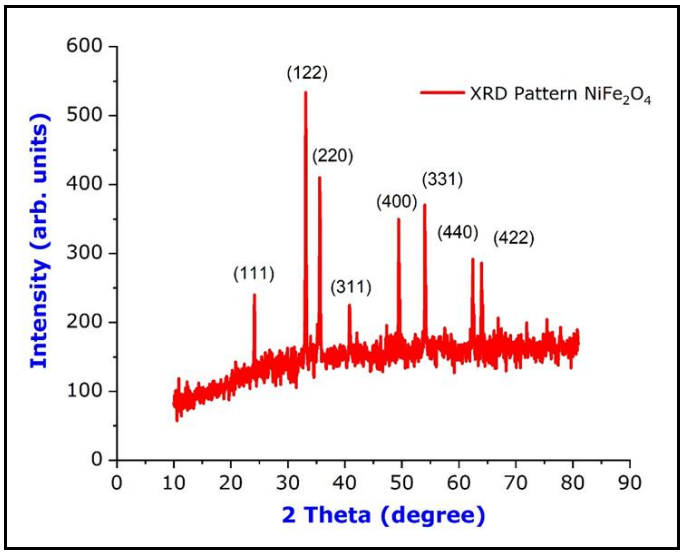

Fig. 1. XRD pattern of $NiFe_2O_4$ nanoparticles

The observed strong diffraction peaks with the (hkl) values in the planes (111), (122), (220), (311), (400), (331), (440) and (422) were perfectly matched available diffraction standard (JCPDS card no: 10-0325) and the crystalline structure was found to be cubic phase [9] and the average particles size of the prepared sample was found as 47 nm by using Debye Scherrer's formula. The presence of strong diffraction peaks with high intensity indicates the crystalline nature of the synthesised sample, which is attributed to the calcination temperature and serves as an indicator of the formation of the zinc ferrite compound [10-12], as reported in the previous literature.

3.2. FTIR spectroscopic analysis

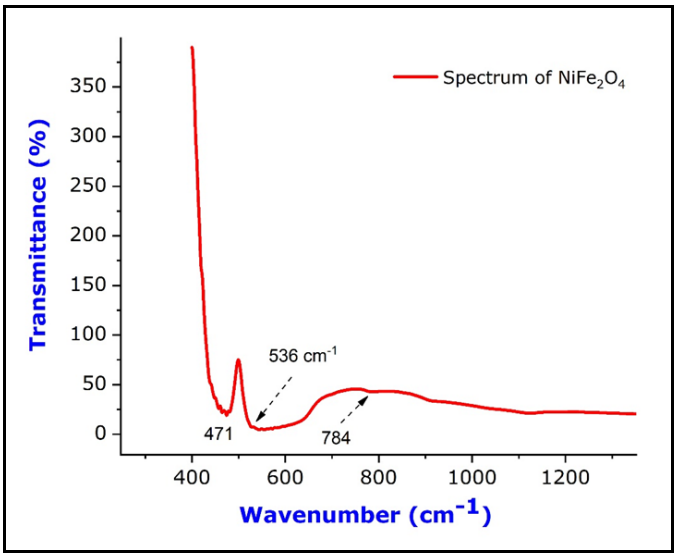

Fig. 2. FTIR spectrum of $NiFe_2O_4$ nanoparticles

To identify the chemical bonding and functional groups present in the prepared $NiFe_2O_4$ nanoparticles, the FTIR spectrum of the synthesised sample was measured, and the functional groups were analysed in the wavelength region of 200 cm^{-1} to 2500 cm^{-1}. The recorded FTIR as shown in Fig. 2. The synthesized $NiFe_2O_4$ nanomaterial which was calcinated at 800 °C revealed the strong absorption peaks in the fingerprint region at 536 cm^{-1} and 471 cm^{-1} which confirms the formation of $NiFe_2O_4$ nanoparticles [13] and it is due to the overlapping of the tetrahedral band in A site and octahedral band in B sites of the sample produced a stretching vibration within the molecules. Also, in this examination, the nonexistence of

the peaks between 1000 - 2500 cm^{-1} and above 3000 cm^{-1} authenticates the absence of O-H, C-O and C=H vibrational bonds of organic substances [14-16]. The unwanted impurities and the nitrites/nitrates or any possible contaminants produced during the reaction from the starting material were completely removed by the high calcination temperature.

3.3. UV-visible spectroscopic analysis

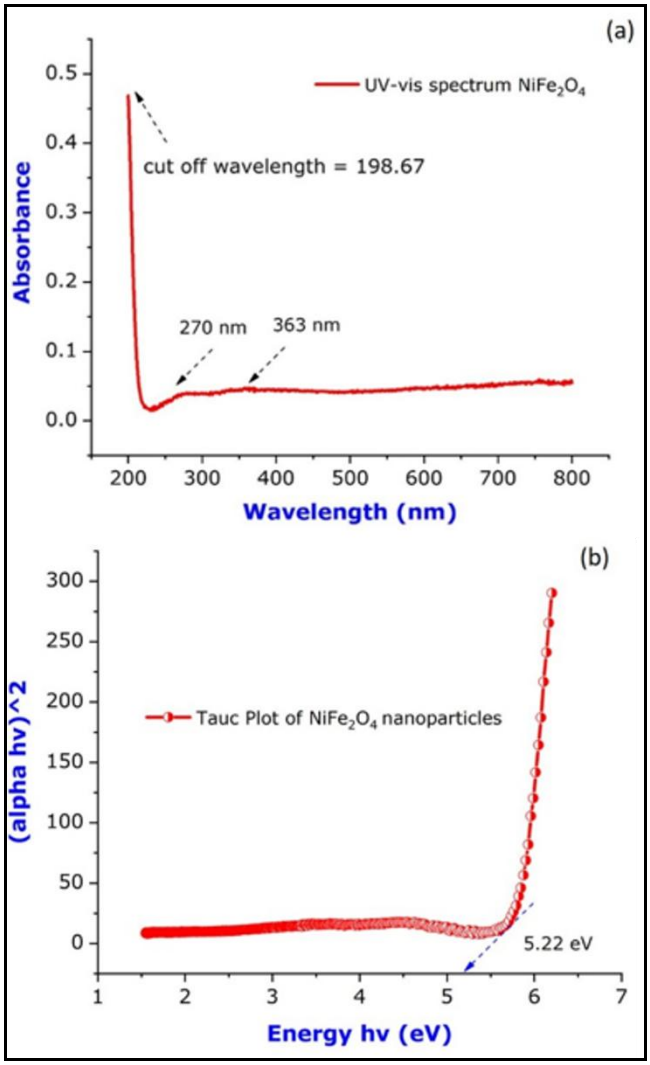

Fig. 3. (a) UV-vis spectrum of $NiFe_2O_4$; (b) Tauc plot of $NiFe_2O_4$ nanoparticles

$NiFe_2O_4$ nanoparticles prepared by the chemical route method were analysed using the UV-vis spectroscopic technique. The absorption spectrum was recorded in the wavelength domain 200 nm – 800 nm as shown in Fig. 3(a-b) [17]. It is observed that the spectral signature for the sample shows an increase in absorption intensity and no shift in the wavelength. The change in the intensity of absorption at 270 nm and 363 nm shows the formation of the bonds between the nickel and iron [18]. Even though considerable variation in the peak absorption position of $NiFe_2O_4$ nanoparticles with particle size was observed, the cut-off wavelength was observed at 198.67 nm. Based on the level of the absorption band, the Tauc plot and using the relation $E_g = hc/\lambda$, the band gap was calculated as 5.22 eV.

3.4. Morphological studies

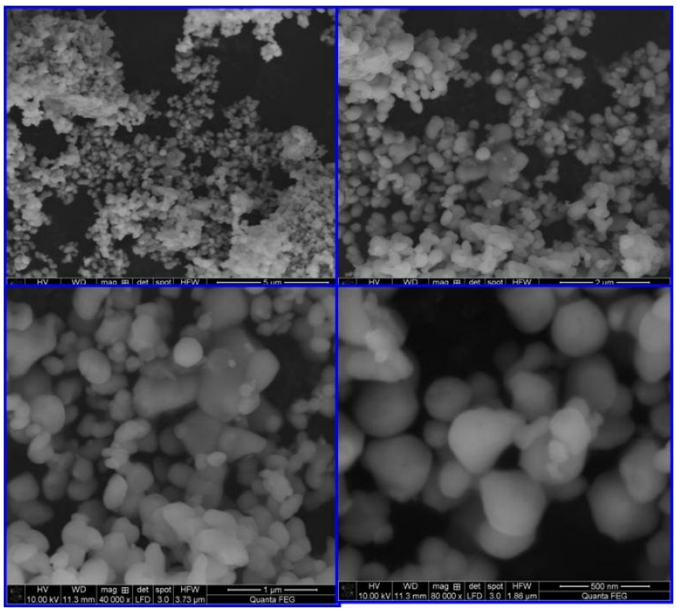

Fig. 4. SEM image of $NiFe_2O_4$ nanoparticles

The SEM images exhibit an agglomerated group of large and tiny spherical nanoparticles and are shown in Fig. 4. The small size of particles leads to high-energy agglomeration due to their high surface energy [19]. The particle distribution is almost homogeneous and spherical

with an average size of 20-60 nanometers. The effect of calcination temperature plays an important role in the configuration of nano-sized ferrite particles [20]. There are reports available in the literature that if the calcination temperature is low, the formation of particles is less and has a reduced reactivity. In this study, we have calcinated the sample at 800 °C, which modified the sample and an almost even spherical distribution of particles was obtained.

3.5. Electrochemical Properties

3.5.1 Complex impedance analysis

Impedance analysis is a significant and unique tool for establishing the dielectric properties of the ferrite materials. Fig. 5(a-b) shows the change in the complex impedance behaviour of the real part and the imaginary part of the impedance with the frequency of the synthesised $NiFe_2O_4$ nanoparticles. From the plot of the real part, it is evident that the impedance decreases with rising frequency for the entire range of temperatures and follows a straight curve in the high-frequency region. Temperature effects in the performance with respect to the applied electric field, especially at low temperature, impedance is maximum and at high temperature, the impedance value is minimum, which can be due to the effect produced by the polarisation of charge carriers in the space between the materials and the electrode [21-23]. A similar trend is followed for the case of the imaginary part. Fig. 5(c) illustrates the frequency and temperature-dependent of the superposed imaginary and real parts of the impedance of $NiFe_2O_4$, in which two overlapping semicircles were obtained for the high temperature.

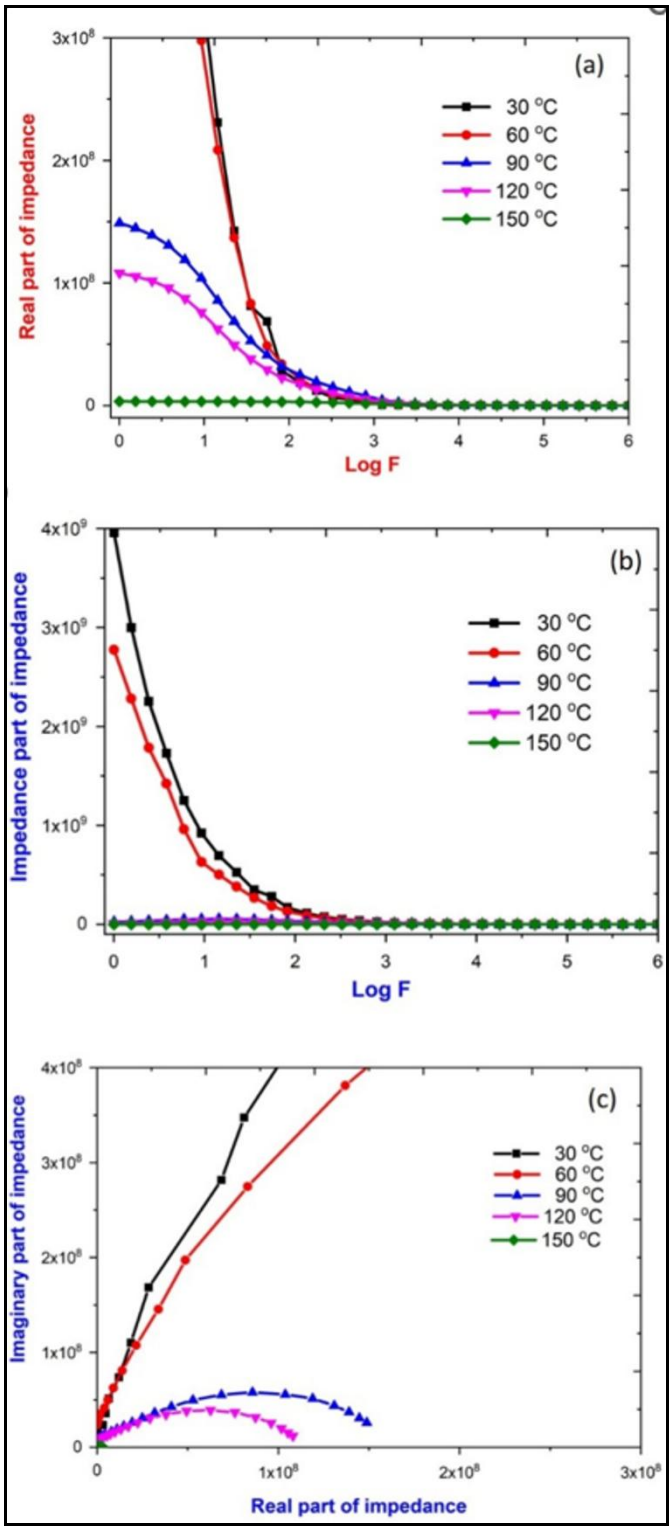

Fig. 5. (a-b) Real and imaginary part of impedance vs frequency; (c) Complex impedance analysis

The decentralisation of the overlapped semicircles is due to the one electrical conductivity mechanism of the ferrite material. At the low-frequency region at high temperatures with a smaller diameter, the electrode dielectric material interface, which creates the hopping motion of the charge carriers between the ions, contributes to the grain boundary and high conductivity [24].

3.5.2 Permittivity

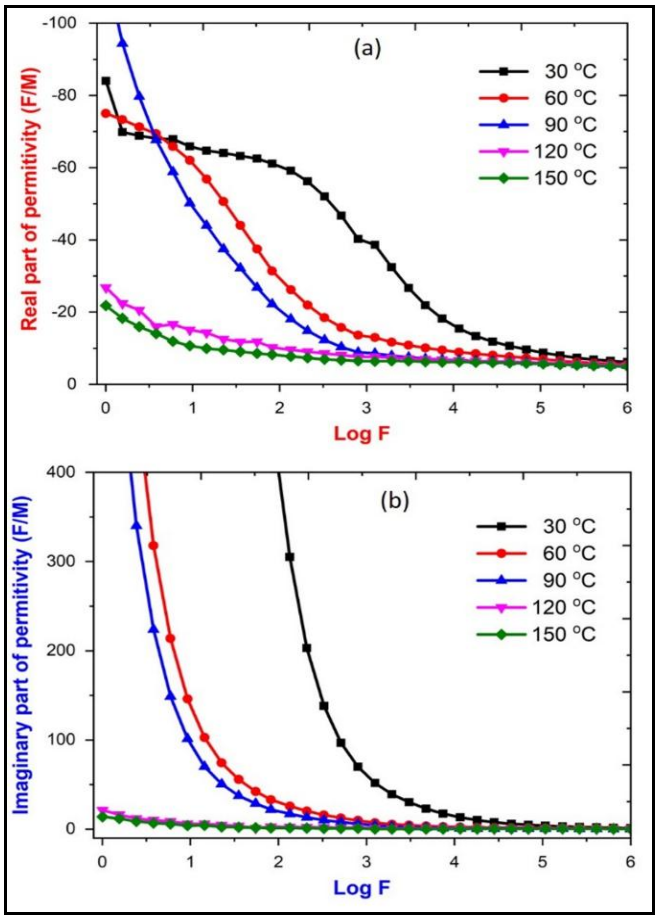

Fig.6.Variation of real and imaginary parts of permittivity with frequency

The permittivity of the synthesised $NiFe_2O_4$ sample with frequency as shown in Fig. 6(a-b). In general, permittivity is a thermodynamic function that depends on the frequency. From the plot, it was observed that in the case of the real part, there is an increasing trend in the low frequency region and a decreasing trend in the mid frequency region, and it may be the ability of the deformation and the relaxation polarizability, which decreases the number of dipoles. A constant trend observed in the high frequency region is due to the rapid polarization which was explained based on the Maxwell-Wagner interfacial polarisation [25]. The distribution varies with temperature. At low frequencies, it is due to ionic relaxation, at the medium frequencies, it is due to dipolar relaxation, and at high frequencies, it is due to atomic and electronic resonances.

3.5.3 Resistivity and ac conductivity at different temperatures

The resistivity and the ac conductivity of the sample $NiFe_2O_4$ are shown in Fig. 7. From the result, it was noted that the resistivity decreases almost exponentially with increasing frequency of the field applied to the sample. And this can be attributed to the increasing effect of the multilayer capacitor according to Koop's theory. It is completely zero at high temperature (150 °C) in the entire frequency range. For medium temperature (90 °C and 120 °C), it was maximum and reached a low value with increasing frequency. At low temperatures (30° and 60 °C), the samples possess high resistivity and approach a minimum in the high frequency, and this type of unpredictable change in the resistivity can be due to the cation's replacement and redistribution of Fe and Ni in their sites, and a narrow independent of temperature and frequency was observed at high frequencies [26].

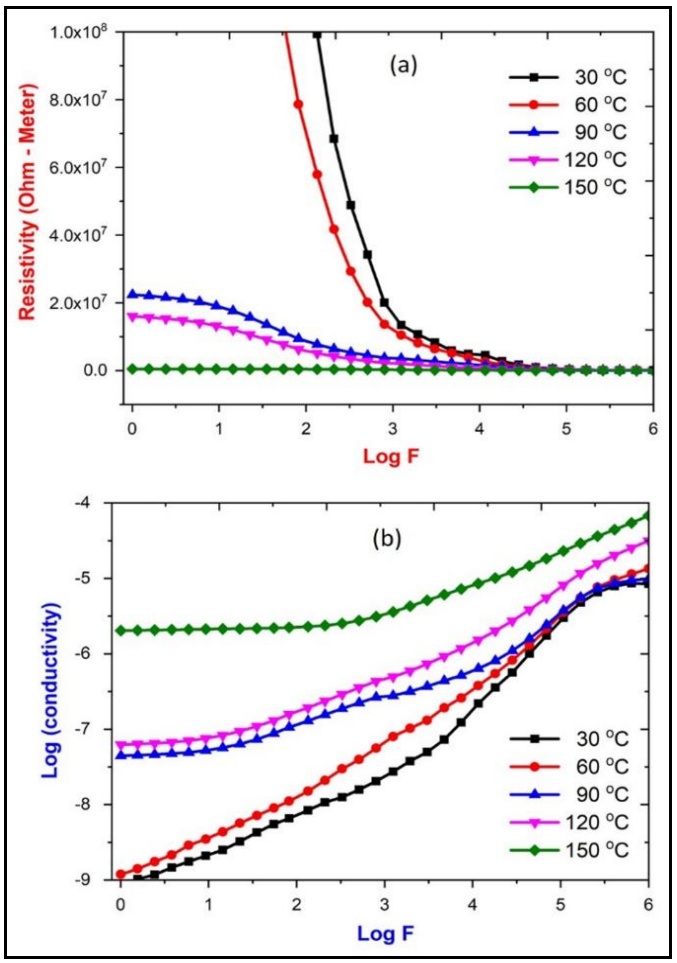

Fig. 7. Variation of resistivity and conductivity with applied frequency

In the case of conductivity, it was observed that the sample possesses high conductivity at high temperature in the entire frequency range, whereas at low temperature, the conductivity of the sample starts to decrease from the high frequency and approaches a minimum at the low frequency.

This poor conductance dependence on frequency, obstinately, the strong dependence of temperature suggests that ferrites are made up of well-conducting grains surrounded by poorly conducting boundaries of grains, which are more active in the low frequencies due to the weak electron hopping

3.5.4 Dielectric constant and dielectric Loss

Dielectric constant and dielectric loss of the synthesised sample are shown in Fig. 8.

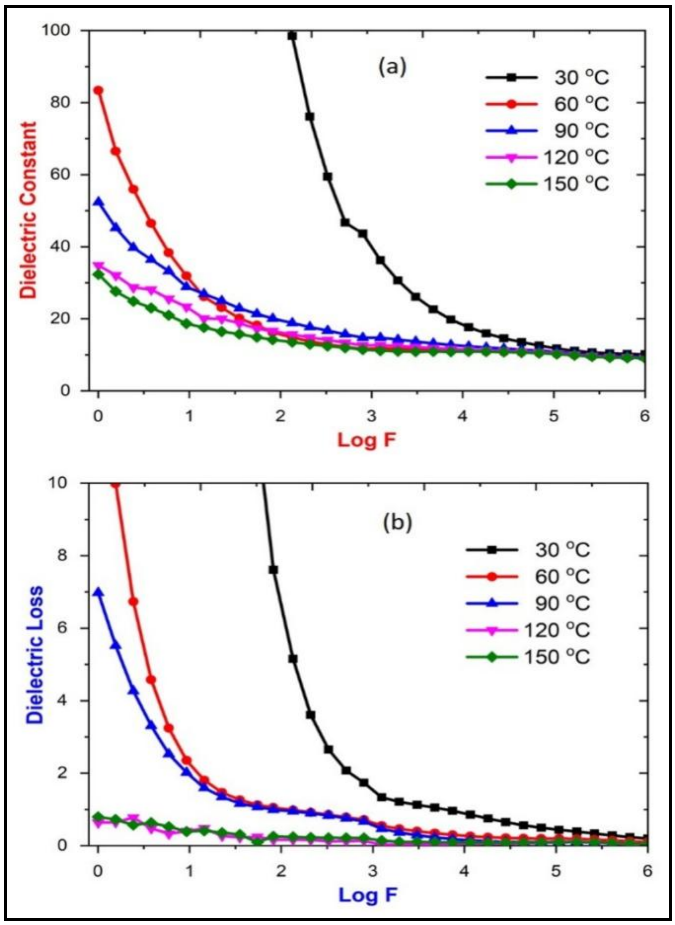

Fig. 8. Dielectric constant and dielectric loss of $NiFe_2O_4$ nanoparticles

From the plot, it was observed that the dielectric constant is very high at low frequencies, which can be due to the interfacial dislocations, creation of oxygen vacancies, charged defects, space charge polarisation of heterogeneous dielectric structure. The decreasing trend of the dielectric constant is rapid in the low frequency region and becomes slower at the higher frequency region, and approaches frequency-independent behaviour. Also, it may be due to the higher conductivity phase in the matrix boundaries of the dielectric [27]. Also, the dipoles do not

follow the rapid variation of alternating fields. The dielectric loss curve showed a rapid decrease in the low and mid frequencies at high temperature. In the high frequency region, it almost becomes frequency independent, and this may be due to the domain wall motions being inhibited, and the forced magnetisation changed the rotation. This variation in dielectric loss is attributed to the concept of space charge polarisation, and high temperature of loss arises due to the macroscopic distribution of charges [28].

3.5.5 Phase Vs Frequency

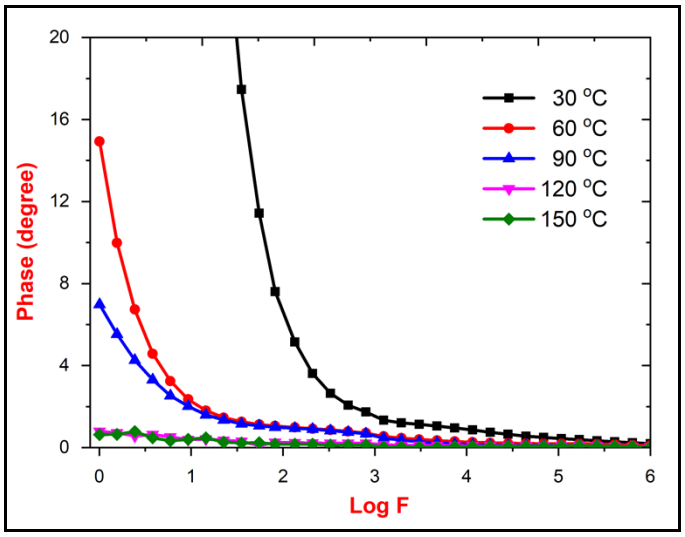

Fig. 9. Phase vs log F of $NiFe_2O_4$ nanoparticles

The dielectric phase angle θ is the angular difference in phase between the alternating potential difference applied to a dielectric and the component of the resulting current, which is generally called as the Bode plot, which explains the absolute impedance and phase angle of the synthesised sample [29]. Change of phase angle with the frequency of the sample $NiFe_2O_4$ is given in Fig. 9. From the results obtained, it was observed that the change in the phase angle decreases towards zero at high temperature. It may be due to the change in the bias voltage, which would change the distribution of interface states at the interfaces and therefore a shift in the capacitance and phase angle.

3.6. Magnetic properties using VSM study

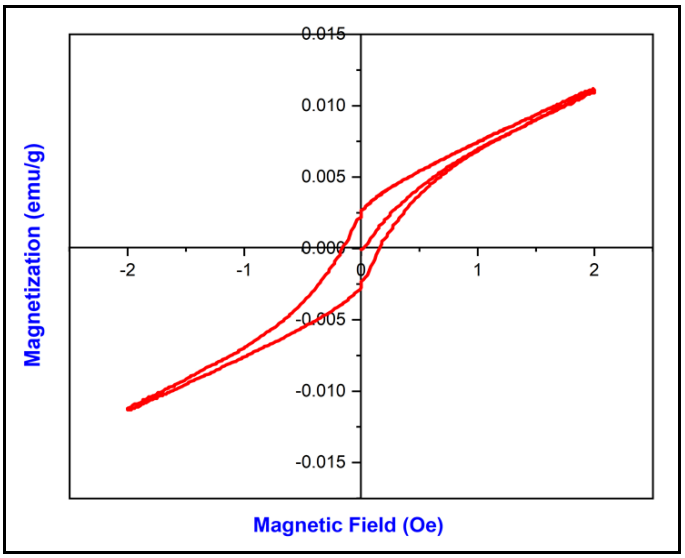

Fig. 10. The ferromagnetic behavior of $NiFe_2O_4$ nanoparticles

The magnetic studies of the synthesised nickel ferrite sample were carried out using a vibration sample magnetometer at room temperature. Fig. 10 shows the hysteresis curves of $NiFe_2O_4$ nanoparticles synthesised by a one-step chemical route method [30,31]. It showed a smaller width hysteresis curve with sharp edges at both ends. The magnetic measurements revealed the nature of the sample and the various parameters calculated, and are found to agree with the previous literature, which showcased the determined values [32,33]. Saturation magnetisation (Ms) was found to be 33.025 emu/g, the remanent magnetisation was found to be 5.63 emu/g, and 56 Oe [34]. The calculated parameters and the behaviour

of the sample indicate the ferromagnetic behaviour [33-35].

4. Conclusion

In summary concluded that nickel ferrite was successfully prepared by the one-step chemical route method. The structural and morphological studies were carried out using XRD and SEM measurements. The presence of Ni and Fe-O bonding was confirmed by using FTIR spectroscopy with robust absorption bands at 536 cm^{-1} and 471 cm^{-1}. The optical bandgap (Eg) was calculated as 5.22 eV using the UV-vis spectroscopic studies. Electrochemical properties like dielectric constant, dielectric loss, impedance, permittivity, conductivity, resistivity, and phase change were studied and measured using dielectric measurements. From the results based on the morphology, dielectric studies and magnetic studies of the sample, this material can find suitable applications in microelectronic devices.

References

1. B. Mahesh, Results Eng. 21, (2024) 101702. B. Mahesh, Results Eng. 21, (2024) 101702.
2. J. Patra, Nano-Struct. Nano-Objects 42, (2025) 101458.
3. S. V. Bhandare, Ceram. Int. 46 (11), (2020) 17400-17415.
4. J. Wan, J. Mater. Chem. 22 (27), (2012) 13500-13505.
5. D. S. Nikam, RSC Adv. 5 (3), (2015) 2338-2345.
6. P. Chauhan, Production of Biobutanol from Biomass, (2023) 255-282.
7. M. M. S. Silva, J. Electroanal. Chem. 933, (2023) 117277.
8. C. D. Langa, Catalysts 15 (8), (2025) 727.
9. M. Parishani, Results Phys. 7, (2017) 3619-3623.
10. E. Umut, J. Colloid Interface Sci. 550, (2019) 199-209.
11. M. K. Anupama, Ceram. Int. 44 (5), (2018) 4946-4954.
12. V. D. Sudheesh, Ceram. Int. 43 (17), (2017) 15002-15009.
13. A. Lassoued, Phys. E Low-Dimens. Syst. Nanostruct. 101, (2018) 212-219.
14. M. R. Ansari, P. Agrohi, and Y. Arya, Next Res. 2 (1), (2025) 100175.
15. R. S. Pandav, J. Magn. Magn. Mater. 417, (2016) 407-412.
16. N. Bouhadouza, Ceram. Int. 41 (9), (2015) 11687-11692.
17. I. Maghsoudi, Powder Technol. 235, (2013) 110-114.
18. M. A. Ahmed, Phys. B Condens. Matter 530, (2018) 195-200.
19. T. Tatarchuk, J. Alloys Compd. 819, (2020) 152945.
20. R. Sharma, Phys. B Condens. Matter 414, (2013) 83-90.
21. C.-H. Lu, Mater. Sci. Eng. B 75 (1), (2000) 38-42. DOI: 10.1016/S0921-5107(00)00386-X

22. T. R. Tatarchuk, J. Alloys Compd. 694, (2017) 777-791. DOI: https://doi.org/10.1016/j.jallcom.2016.10.067
23. B. R. Babu, Mater. Chem. Phys. 207, (2018) 534-541. DOI: https://doi.org/10.1016/j.matchemphys.2017.12.084
24. T. Shanmugavel, J. King Saud Univ. Sci. 27 (2), (2015) 176-181. DOI: 10.1016/j.jksus.2014.12.006
25. A. Manohar, Mater. Chem. Phys. 192, (2017) 235-243. DOI: https://doi.org/10.1016/j.matchemphys.2017.01.039
26. L. Kumar, J. Magn. Magn. Mater. 323 (15), (2011) 2042-2048. DOI: https://doi.org/10.1016/j.jmmm.2011.03.010
27. P. B. Belavi, Mater. Chem. Phys. 132 (1), (2012) 138-144. DOI: https://doi.org/10.1016/j.matchemphys.2011.11.009
28. A. Dhayal Raj, Curr. Appl. Phys. 10 (2), (2010) 531-537. DOI: https://doi.org/10.1016/j.cap.2009.07.015
29. N. M. Basith, Mater. Sci. Semicond. Process. 17, (2014) 110-118. DOI: https://doi.org/10.1016/j.mssp.2013.09.013
30. T. Prakash, J. Alloys Compd. 667, (2016) 255-261. DOI:https://doi.org/10.1016/j.jallcom.2016.01.172
31. K. Poovendran, Surf. Interfaces 19, (2020) 100474. DOI: 10.1016/j.surfin.2020.100474
32. J. Guo, RSC Adv. 7 (72), (2017) 45420-45431. DOI:10.1039/C7RA08781K
33. K. Kombaiah, Mater. Chem. Phys. 221, (2019) 1128. DOI: https://doi.org/10.1016/j.matchemphys.2018.09.012
34. A. M. Amanulla, Surf. Interfaces 22, (2021) 100835. DOI: 0.1016/j.surfin.2020.100835
35. S. B. Gopale, J. Phys. Conf. Ser. 1644 (1), (2020). DOI:10.1088/1742-6596/1644/1/012003